NAR Cancer, 2025, **7**, zcaf005
https://doi.org/10.1093/narcan/zcaf005
Advance access publication date: 18 February 2025
Nucleic Acid-Based Cancer Therapeutics

In vivo selection of anti-glioblastoma DNA aptamers in an orthotopic patient-derived xenograft model

Caroline D. Doherty[1], Brandon A. Wilbanks[2], Sonia Jain[3], Keenan S. Pearson[2], Katie K. Bakken[3], Danielle M. Burgenske[3], Nay Won Lett[2,4], Jann N. Sarkaria[2,3], Louis J. Maher, III[2,*]

[1]Department of Molecular Pharmacology and Experimental Therapeutics, Mayo Clinic Graduate School of Biomedical Sciences, Rochester, MN 55905, United States
[2]Department of Biochemistry and Molecular Biology, Mayo Clinic Graduate School of Biomedical Sciences, Rochester, MN 55905, United States
[3]Department of Radiation Oncology, Mayo Clinic, Rochester, MN 55905, United States
[4]Summer Undergraduate Research Fellowship, Mount Holyoke College, South Hadley, MA, 01075 United States
[*]To whom correspondence should be addressed. Email: maher@mayo.edu

Abstract

Glioblastoma (GBM) is the most common and aggressive primary malignant brain tumor of adults. Current therapeutic options yield dismal prognoses that have remained essentially unchanged over nearly two decades. Diffuse growth patterns, high intratumoral heterogeneity, and variable blood–brain barrier integrity limit treatment efficacy, creating challenges that rational small molecule design has not overcome. Antibody–drug conjugates have shown some promise, leading us to hypothesize that smaller folded DNA aptamers, developed *in vivo* via principles of natural selection, might eventually have advantages for drug delivery. Here, we document the first *in vivo* DNA aptamer selection involving an orthotopic patient-derived xenograft GBM mouse model to identify tumor-homing DNA aptamers. We demonstrate the preferential accumulation of these aptamers in the tumor relative to other tissues 4 h after intraperitoneal injection. The aptamers can be detected by quantitative polymerase chain reaction, fluorescent tumor staining, and stain GBM tumor section from untreated mice and the GBM tumor cells in culture. Two of three candidates are selective for the target cell line *in vitro* and do not bind other human tumor cells. *In vivo* selection of tumor-specific DNA aptamers demonstrates a novel approach for diagnostics or toxin delivery that might allow for the development of individualized therapies.

Graphical abstract

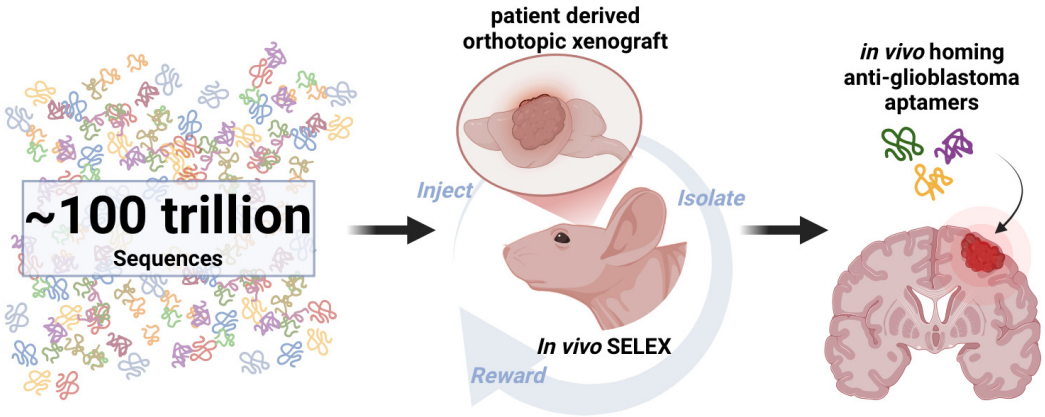

Introduction

Glioblastoma (GBM) is a primary central nervous system malignant brain tumor that accounts for nearly 50% of primary metastatic brain tumors in adults [1]. With a dismal 5-year survival rate of <10%, the prognosis for GBM patients has remained essentially unchanged for nearly two decades since temozolomide therapy was approved in 2005 [2, 3]. Unlike other tumors in which improved understanding of cancer pathobiology has led to highly effective targeted therapies, this translation has been absent in GBM [4]. This failure is often attributed to inherent high intratumoral heterogeneity and challenges in therapeutic delivery, such as delivery across the blood–brain barrier (BBB) [5–7]. Antibody–drug conjugates (ADCs) have shown some promise,

Received: October 24, 2024. **Revised:** January 24, 2025. **Editorial Decision:** January 29, 2025. **Accepted:** February 3, 2025

but their large size limits BBB penetration and therapeutic efficacy [8].

Aptamers are short, folded single strands of synthetic DNA or RNA and have been explored as BBB-penetrating agents [9]. As single-stranded nucleic acid polymers, aptamers fold into unique three-dimensional shapes and act as antibody analogs, binding targets with dissociation constant (K_d) values in the nanomolar range [10]. Unlike other nucleic acid-based therapies, the functionality of aptamers is derived from their three-dimensional shape rather than genetic coding. Aptamers are identified through Systematic Evolution of Ligands by Exponential enrichment (SELEX). This process is based on the principles of natural selection, in which an aptamer library of hundreds of trillions of unique shapes is introduced to a target of interest and allowed a set time for target-specific binding. Molecules that successfully reach the target are "rewarded" with polymerase chain reaction (PCR) amplification and serve as the library for the next round of selection, while nonspecific molecules are removed. This cycle is repeated until enrichment in the library is observed. Targets range from purified molecules, such as proteins, to cells or complex tissues. Various SELEX strategies are commonly used to develop aptamers for applications, including therapeutics, biomarker discovery, and diagnostics [11–14]. Importantly, aptamer development *ex vivo* may identify molecules that do not function optimally *in vivo* where complex pharmacokinetic principles, such as persistence in circulation and correct compartment delivery, may prevent adequate accumulation within a target tissue.

We hypothesized that selection of GBM-homing aptamers could be accomplished by *in vivo* SELEX to isolate candidates with the potential to overcome current therapeutic delivery challenges. The challenges of rationally designing a small molecule toxin to cross the BBB, enter the brain parenchyma, and differentiate tumor from nontumor are inherently incorporated into the *in vivo* SELEX. In doing so, candidates are selected for their ability to solve these problems *in vivo*. Selected aptamers could create therapeutic leads, while also illuminating molecular mechanisms of BBB penetration and GBM targeting. *In vivo* SELEX therefore has the potential to address simultaneously the optimization of bioavailability, biodistribution, stability, and rapid target tissue delivery. *In vivo* SELEX has been described in a limited number of reports, but applications in neuro-oncology have not been attempted [15]. While aptamers developed for other indications, such as olaptesed pegol (NOX-A12), are entering GBM clinical trials and showing promising safety and efficacy, developing novel methods to effectively select aptamers for neuro-oncology applications is crucial [16–18].

Here, we report the first *in vivo* SELEX approach relevant to neuro-oncology: targeting an orthotopic patient-derived xenograft (PDX) brain tumor model in mice [15]. We demonstrate that an orthotopic PDX mouse model can be used for *in vivo* SELEX that successfully identifies multiple GBM tumor-homing aptamers after eight rounds of selection. Elucidation of the biodistribution of three of the resulting aptamers demonstrates significant tumor preference. We show that the selected aptamers are not more stable in blood but have been selected for tumor homing as detected by both fluorescence detection and quantitative PCR (qPCR). *In vitro* characterization demonstrates that two of the candidate aptamers associate with the PDX cell line against which they were selected, but do not recognize other human cell lines. Thus, these studies demonstrate the ability of *in vivo* SELEX to generate libraries of DNA aptamers that rapidly home to GBM tumors in the brain. This work has implications for both diagnostics and the development of individualized aptamer–drug conjugates.

Materials and methods

Naïve random DNA library synthesis for *in vivo* SELEX

DNA oligonucleotides (Supplementary Table S1) were obtained from Integrated DNA Technologies (IDT). Forward and reverse primers used during SELEX were synthesized with 5′-fluorescein (5′-FAM) and an internal nine-atom triethylene glycol spacer, respectively, the latter acting as a non-extendable linker enabling separation of aptamer from complementary strands during denaturing electrophoretic gel purification. The library was constructed with two constant 20-nucleotide primer regions flanking 40 random nucleotides. All oligonucleotides were reconstituted at 100 μM. Primers were diluted to 5 μM. For selection round 1, the naïve DNA library was substituted with 5-methyl-deoxycytidine (5mdC) outside of the forward primer region by PCR using the following reagent volumes in a master mix: 400 μl of 10× *Taq* polymerase buffer, 400 μl of 10× bovine serum albumin (BSA), 320 μl of 50 mM $MgCl_2$, 320 μl of 2.5 mM dNTPs (2.5 mM 5-methyl-dCTP, dATP, dGTP, and dTTP), 100 μl of 1 μM library DNA, 400 μl of 5 μM forward primer, 400 μl of 5 μM reverse primer, 1460 μl water, and 50 μl *Taq* DNA polymerase (Invitrogen, #10342020). Reagents were mixed, aliquoted into 100 μl volumes in PCR tubes, and subjected to thermal cycling for a variable number of cycles using the following protocol: 95°C, 60 s; 25× (94°C, 15 s; 50°C, 35 s; and 72°C, 30 s); 4°C. DNA was amplified for only three cycles before round 1 to incorporate base modifications while minimizing PCR bias and maintaining library diversity.

PCR reactions were pooled (4 ml) and precipitated from 2.5 volumes of ethanol after addition of glycogen carrier and sodium acetate to a final concentration of 0.3 M. After washing with 70% ethanol and air drying, PCR products were resuspended in water and deionized formamide (Ambion, #AM9342), heated at 90°C for 5 min, and subjected to electrophoresis through a 10% polyacrylamide gel [7.5 M urea, 19:1 acrylamide:bisacrylamide (Bio-Rad, #1610144)] at 200 V for 2 h. As the reverse primer had an additional 20-nucleotide non-extendable linker (Supplementary Table S2), the reverse strand was 20 nucleotides heavier in molecular weight, permitting clear separation of the forward and reverse strands (Supplementary Fig. S1). FAM-labeled DNA bands (aptamer library strand) were visualized by UV shadowing, excised with a razor blade, diced, and incubated in 2× PK buffer [100 mM Tris–Cl (pH 7.5), 200 mM NaCl, 2 mM ethylenediaminetetraacetic acid, and 1% sodium dodecyl sulfate] at 56°C with agitation overnight. Eluted DNA was collected and purified by phenol:chloroform (VWR, #97064-692) extraction and ethanol precipitated as described earlier. The concentration of the resulting naïve library was determined with a NanoDrop instrument at 260 nm using a library-specific estimated extinction coefficient [754 075 l/(mol cm)]. A 1 μM aptamer dosing solution in phosphate-buffered saline (PBS) and 1 mM $MgCl_2$ (250 pmol aptamer/250 μl) was created from the purified material.

PDX models

Short-term explants of PDX were obtained from the Mayo Clinic Brain Tumor Patient-Derived Xenograft National Resource. PDXs were established directly from patient biopsy or surgical samples as flank tumors on athymic nude mice and maintained as previously described [19]. These tumors were then used to establish short-term explant cultures or intracranial xenografts [19]. Each PDX model is highly annotated with multi-omics characterization and relevant clinical data as previously described [20].

Mice

Female athymic nude (strain #553) mice were purchased from Charles River Laboratories. All animal experiments were approved by Mayo Clinic Institutional Animal Care and Use Committee, Protocol #A00006585-22. Orthotopic tumor inoculation and bioluminescence imaging (BLI) were performed as previously described [8, 19].

Cell culture

GBM PDX lines were maintained as previously described [20]. Short-term explant cultures of GBM6, GBM10, GBM14, GBM39, GBM43, and GBM108 PDX, and U87 glioma (ATCC, #HTB-11), HeLa (ATCC, #CCL-2), A549 (ATCC, #CCL-185), U2OS (ATCC, #HTB-96), and MCF7 (ATCC, #HTB-22) cell lines were grown in Dulbecco's modified Eagle medium (DMEM; Fisher Scientific, #MT10013CV), supplemented with 10% fetal bovine serum (FBS; Gibco, #220346) and 1% penicillin/streptomycin (Life Technologies, #221674) at 37°C and 5% CO_2. Identities of PDX and U87 lines were verified by short tandem repeat analysis. PDX lines were tested every 6 months for mycoplasma using a MycoAlert mycoplasma detection kit (Lonza, #LT07-418).

In vivo SELEX in orthotopic PDX mice

Prior to SELEX, nine mice were injected with explants of GBM39-eGFP-FLUC2 cells in three groups (three mice per group) with the following cell counts: 100 000, 10 000, or 1000 cells, to distribute tumor development over time. Tumor development was monitored by BLI (IVIS Spectrum). Once the tumor reached a BLI reading between 5×10^8 and 1×10^9, the mouse was enrolled for a round of *in vivo* SELEX.

On the day of selection, one mouse received an intraperitoneal (i.p.) injection of 250 pmol aptamer library in 250 µl PBS containing 1 mM $MgCl_2$. Four hours post-injection, the mouse was euthanized with CO_2 and subjected to scrupulous transcardial perfusion with 30–60 ml PBS as follows: the euthanized mouse was pinned outstretched at a vertical angle and a 21g × 1″ needle was inserted into the left ventricle while the heart was still beating. The mouse was perfused until the liver changed from dark red to pale brown with the effluent gravitationally pooling below the mouse. The brain was extracted, and the tumor was dissected with the aid of fluorescent goggles. Adjacent brain, and normal heart, lungs, liver, kidneys, and spinal cord were also extracted and snap-frozen. Bone marrow was extracted by flushing the femur with 5 ml PBS, centrifugation at 1250 rpm for 5 min, removing the supernatant, and weighing the resulting bone marrow pellet before freezing. For each selection round, aptamers were extracted from the PDX tumor using a modified Qiagen Plasmid Extraction Kit protocol. The tumor was thawed on ice and homogenized with a plastic pestle in 300 µl Buffer P1. To this, 300 µl of Buffer P2 was added followed by gentle mixing by inversion and then incubation at room temperature for 5 min, followed by addition of 300 µl Buffer P3. The solution was mixed by gentle inversion until a white precipitate was observed. The sample was incubated on ice for 10 min and then subjected to centrifugation at 13.3 krpm for 10 min in a microcentrifuge. The supernatant was added to 60 µl of proteinase K (10 mg/ml) solution and incubated at 55°C overnight. The resulting solution was purified by phenol:chloroform extraction (800 µl of 25:24:1 phenol:chloroform:isoamyl alcohol) followed by precipitation with an equal volume of isopropanol. The crude DNA pellet was air dried for 10 min and then resuspended in 50 µl water.

A 15 µl sample of this crude solution containing tumor-isolated aptamer was added to a 3.2 ml PCR reaction mix composed of 320 µl of 10× *Taq* polymerase buffer, 320 µl of 10× BSA, 256 µl of 50 mM $MgCl_2$, 256 µl of 2.5 mM dNTPs (2.5 mM 5-methyl-dCTP, dATP, dGTP, and dTTP), 320 µl of 5 µM forward primer, 320 µl of 5 µM reverse primer, 1348 µl water, and 45 µl *Taq* DNA polymerase (Invitrogen, #10342020). From this, seven aliquots (20 µl each) were used for cycle optimization. Samples (20 µl) were removed at cycles 13, 16, 19, 22, 24, 27, and 30, and the optimal number of cycles was determined by the homogeneity and yield of the PCR product band and consumption of primers analyzed on a denaturing 10% polyacrylamide gel. The remaining volume was PCR amplified at the optimal number of cycles determined for that round (usually around 30 cycles). PCR reactions were pooled, precipitated from ethanol after addition of NaOAc and glycogen as before, and resuspended in 60 µl water. The resulting sample was prepared for denaturing gel purification by addition of 4 volumes of deionized formamide, mixing, and heating at 90°C for 5 min. Samples were loaded onto a prerun 10% denaturing polyacrylamide gel (60 µl per lane) and subjected to electrophoresis at 600 V for 2 h. The forward FAM-labeled strand was visualized with a UV lamp and excised with a fresh razor blade. This band was diced and transferred to microcentrifuge tubes with 450 µl of 2× PK buffer and incubated overnight at 56°C with agitation at 1500 rpm. DNA was then extracted using 1:1 phenol:chloroform, precipitated from ethanol as before, and resuspended in 60 µl water. The absorbance at 260 nm (NanoDrop) was divided by the molar extinction coefficient to calculate the concentration of the recovered library. The sample for the next round of selection was prepared by adding 25 µl of 10× PBS and 2.5 µl of 250 pmol library, and increasing the volume to 250 µl. This cycle was repeated for each round of selection.

Aptamer sequencing

The naïve oligonucleotide library containing 5-methyl-dC, the libraries from eight selection rounds, and aptamers extracted from all tissues in the round 8 mouse were subjected to deep sequencing. Gel-purified material was used in each case. Libraries were amplified for the number of cycles determined by analytical PCR in each selection round using unmodified primers. PCR reactions contained 10 µl of 10× *Taq* DNA polymerase buffer, 10 µl of 10× 1 mg/ml BSA, 8 µl of 50 mM $MgCl_2$, 8 µl of 2.5 mM dNTPs, 10 µl library, 10 µl of 5 µM forward primer, 10 µl of 5 µM reverse primer, 32.6 µl water, and 1.4 µl *Taq* DNA polymerase. PCR product size and quality were confirmed by electrophoresis through an 8% native

polyacrylamide gel (29:1 acrylamide:bisacrylamide; Bio-Rad, #1610146).

PCR products were purified with the Qiagen MinElute Purification Kit (Qiagen, #28004). Ten nanograms of eluted DNA, as quantified by the Qubit HS Duplex DNA Quantification Kit (Invitrogen, #Q32851), was used as input for the NEBNext Ultra II DNA Library Prep Kit (NEB, #E7645S) using associated NEBNext Multiplex primer index (primer sets 1 and 2; NEB, E7335S and E7500S). After preparing samples according to the manufacturer's instructions (recommended volumes were halved and in the purification of adaptor ligated DNA Qiagen MinElute Purification Kit was used instead of beads), samples were assessed by gel electrophoresis through an 8% native polyacrylamide get (29:1 acrylamide:bisacrylamide) prior to analysis by high-throughput paired-end 150-cycle sequencing on a single lane of an Illumina MiSeq instrument (Mayo Clinic Sequencing Core).

Sequencing files were received as .bam and converted to .fastq files. Usearch was used to first merge paired-end reads. The merge files were filtered using the usearch maxee function, discarding files with errors >0.5. Reverse strands were isolated, and the reverse complements created using SeqKit reverse complement tool. The two files were combined with the simple concatenate function in Linux. AptaSUITE was used to filter any reads that did not contain both forward and reverse primers within an error of three bases, and rank aptamers by sequence or cluster abundance [21].

Following deep sequencing analysis, aptamer enrichment was analyzed by identifying the most prevalent sequences and sequence clusters and by determining area under the curve of all sequences identified at round 8. Individual candidate aptamers were then synthesized by IDT with 5-methyl-dC substitutions and 5′-FAM modifications.

Cell binding assays

For all cell association experiments, explants of the parental G39 line (lacking eGFP) were used. Cells were plated in 12-well plates (Corning, #3512) overnight or for 72 h. Cells were ∼80% confluent on the day of the experiment. Cells were washed with wash buffer (PBS containing 1 mM $MgCl_2$ and 4.5 g/l glucose) prior to adding 200 nM of heated and snap-cooled aptamer in selection buffer (1 mM $MgCl_2$ in PBS) with 4.5 g/l glucose, 100 μg/ml sheared salmon sperm (Invitrogen, #15632011V), and BSA (New England Biolabs, #B9200S). Cells incubated with the indicated concentrations of aptamers for 1 h at 37°C. Cells were washed with wash buffer three times prior to fixation with 3.7% formaldehyde for 15 min. Cells were stained with anti-FAM antibody (Invitrogen, #A11090) for 1 h at room temperature followed by three washes with wash buffer and staining with secondary antibody conjugated to AF647 (Invitrogen, #A32733) for 1 h at room temperature. The cells were washed three times prior to imaging in an Incucyte instrument (SX5, Sartorius). Staining and confluence were calculated as determined by Incucyte software.

For cell binding determination by qPCR, cells were plated in 24-well plates. The cell binding protocol was followed as above with three replicates per condition. However, rather than fixation, cells were recovered by scraping on ice, collected, and the well was washed with wash buffer once to collect any remaining cells. The cells were heated at 95°C for 10 min and then subjected to centrifugation at 13 100 × *g* in a microcentrifuge. The supernatant was used for qPCR (QuantaBio PerfeCTa, #95071-012). Protein was quantified as determined by Qubit Protein Assay Kit (Invitrogen, #Q33211).

Analysis of individual aptamer biodistribution

Mice were stereotactically injected with 100 000 parental GBM39 without GFP expression, as described earlier. Mice were closely monitored for weight and behavioral changes as signs of tumor progression. Animals approaching moribund status were enrolled in the study. Aptamer cocktail solutions of 200 pmol/250 μl (50 pmol each aptamer) were created in PBS containing 1 mM $MgCl_2$, heated for 5 min at 90°C, and snap-cooled on ice for 10 min. Control vehicle solutions lacking aptamers were created at the same time. Mice were injected i.p. with 250 μl aptamer cocktail (200 pmol) or vehicle. Four hours post-injection, mice were euthanized, underwent scrupulous transcardial perfusion as described earlier, and the brain, heart, lungs, spleen, liver, kidneys, bone marrow, and sciatic nerve were removed. The bone marrow was collected from both femurs by centrifugation at ≥10 000 × *g*. All tissues were snap-frozen on dry ice and stored at −80° C.

Brain dissection involved warming the brain to −20° C and placement in a dissection block at this temperature. Fresh razor blades were placed as indicated in Fig. 2A and Supplementary Fig. S5D. Two 1-mm sections were obtained and stained with toluidine blue (0.33 mg/ml) for 30 s. Excess toluidine blue was removed from the tissue and the brain was dissected away from the tumor using differential toluidine blue staining of tumor tissue as a guide. After sectioning was complete, the remaining posterior tumor was dissected from the right hemisphere. The cerebellum was isolated. All tissues were placed in tared tubes and immediately frozen on dry ice. Similarly, all organs were transferred to tared tubes.

For biodistribution experiments, an optimized aptamer extraction method maximized yield as indicated in Supplementary Fig. S4. This protocol is recommended for future *in vivo* SELEX experiments. Samples <200 mg were homogenized in 300 μl Qiagen Plasmid Extraction Kit Buffer P1 with a plastic pestle and placed on ice. Lysis buffer (300 μl: 50 mM Tris–HCl, pH 7.4, 150 mM NaCl, 1% NP-40, 0.5% sodium deoxycholate, 1 mM EGTA (ethylene glycol-bis(β-aminoethyl ether)-*N,N,N',N'*-tetraacetic acid), and 1 mM NaF) was then added and the sample was vortexed to mix. Samples were incubated on ice for at least 1 h prior to sonication at power 8 (Sonic Dismembrator 60, Fisher Scientific) for 10 s three times with 30 s of cooling on ice between treatments. Samples were heated to 95°C for 10 min and subjected to centrifugation at 13,100 × *g* for 5 min. The supernatant was removed and analyzed by qPCR as described earlier.

Immunofluorescence detection of injected aptamer

Nude mice bearing GBM39 tumors were injected with 250 pmol aptamer E or X, and were euthanized 4 h post-injection, thoroughly perfused as described, and brains removed and frozen in optimal cutting temperature (OCT) solution (Tissue-Tek, #4583). Five-micrometer tissue sections were applied to slides, dried for 10 min, and washed once with PBS. Slides were fixed with fresh 4% paraformaldehyde (PFA) for 15 min and washed once prior to permeabilization with 0.1% Triton X-100 for 10 min. Slides were washed three times with PBS

and a Pap Pen was used to trace specimen perimeters. Slides were mounted by adding 1–3 drops of 4', 6-diamidino-2-phenylindole (DAPI) mounting media (Invitrogen, #P36980) to the section, adding a coverslip, and sealing with nail polish.

Tumor detection by aptamers *ex vivo*

For aptamer staining of GBM tumor *in situ*, 5-μm sections of paraffin-embedded brain from untreated mice carrying GBM39 PDX tumors were used. The tissue was preblocked with 10% goat serum and 2% BSA in PBS for 1 h at room temperature prior to addition of anti-FITC antibody (Invitrogen, #A11090) 1:500 dilution in 2% goat serum with 2% BSA in PBS overnight in a humidified box. Sections were washed with PBS four times. Anti-rabbit antibody conjugated to AF647 (Invitrogen, #A32733) was added at a dilution of 1:500 in 2% serum with 2% BSA in PBS for 1 h at room temperature in the dark. Sections were washed four times with PBS and the slides were mounted and stained with DAPI as described earlier. Unless specified, all steps were performed at room temperature.

Aptamer stability in serum

Heated and snap-cooled aptamer at 1 μM concentration was added to FBS at a final concentration of 1 pmol/100 μl. Samples were incubated at 37°C for up to 6 h with agitation. Samples were collected at 0, 0.5, 1, 2, 4, and 6 h and diluted 1:1 with lysis buffer. Samples were then heated at 95°C for 10 min prior to centrifugation at 13,100 × *g* for 5 min. Supernatants were analyzed by qPCR analysis as described earlier.

Toxicity analysis

A CellTiter-Glo assay (Promega, #G7571) was used to determine aptamer toxicity. Aptamers were mixed with complete media and added to GBM39 cells. Six days post-treatment, the CellTiter-Glo assay was performed according to the manufacturer's protocol.

Results

In vivo selection of DNA aptamers localizing to orthotopic patient-derived GBM tumors

In vivo selection was performed using athymic nude mice bearing orthotopic PDX brain tumors as outlined in Fig. 1A. GBM39 was harvested from a 51-year-old male with a confirmed left frontal glioblastoma, IDH-wildtype tumor and implanted directly into mice as previously described [19]. Mice were implanted with explants of the tagged PDX line GBM39-eGFP/fLuc2 and tumor growth was monitored by BLI until readings between 5×10^8 and 1×10^9 log total flux were observed. On the day of selection, one mouse received an i.p. injection of 250 pmol aptamer library ($\sim 10^{14}$ aptamers with 40 random positions flanked by known 20-nucleotide sequences enabling PCR). Aptamers carried 5′-FAM tracers and all deoxycytosine residues were replaced by 5-methyl-deoxyctytosine with the intent to minimize any innate immune recognition of unmethylated 5′-CpG dinucleotides in the DNA strands. Four hours were allowed for aptamer circulation with the goal that properly folded aptamers would reach the brain parenchyma, cross the BBB, and accumulate in the GBM tumor by any available mechanisms. The mouse was then euthanized and thoroughly perfused with saline to remove aptamers present in blood vessels. The tumor was isolated by monitoring GFP signal, and recovered aptamers were amplified by PCR incorporating 5mdC outside of the forward primer region (designed without CpG dinucleotides). Selection progress was monitored by qPCR recovery from the tissue (Supplementary Fig. S2A and B). Recovered DNA was subjected to deep sequencing following eight rounds of selection. Sequences were sorted into clusters, which were defined as sequences within two nucleotides from the cluster seed sequence [21]. Cluster variants likely result from low levels of *Taq* DNA polymerase mutagenesis. Interestingly, the top enriched clusters represented <0.015% of the recovered pool (Fig. 1B), significantly lower than we typically observe for eight rounds of less stringent cell- or protein-targeted selections. We chose three candidates for further testing. Aptamers E, B, and A are the cluster seeds for clusters (i), (ii), and (v), respectively. Aptamer A was chosen as the most enriched individual sequence in round 8 (Supplementary Fig. S2C), aptamer E was chosen as the cluster seed of the most enriched cluster (ii) in round 8 (Fig. 1B), and aptamer B was chosen as the second most abundant sequence and cluster judged by area under the curve over eight selection rounds (Fig. 1B). The negative control sequence (X) was randomly selected from sequences present in the naïve library but not present in the round 8 library.

Aptamers extracted from the surrounding brain, posterior left hemisphere, heart, kidney, liver, lung, and spinal cord in the mouse at round 8 were also subjected to deep sequencing to enable biodistribution measurements (Fig. 1C and D). The clusters represented by all three selected candidate aptamers demonstrated strong tumor preference relative to other tissues. While this was a favorable initial indication of GBM homing, many of these organs demonstrated only tens of candidate sequence reads per sample. Thus, studying larger doses of the candidates was important.

The secondary structures of the candidates and negative control were predicted using Mfold software under folding buffer conditions (Na^+ and Mg^{2+} concentrations of 153 and 1 mM at 24°C, respectively; Fig. 1E) [22, 23]. Interestingly, the lowest-energy predicted secondary structures for the three selected candidates shared similar organization of 5′ and 3′ fixed sequences, whereas the negative control did not (Supplementary Fig. S2D and E).

Accumulation of aptamers in tumor and tissues

Given the relatively low candidate recovery in the round 8 selection pool, we next verified that aptamer tumor localization was detectable by methods other than deep sequencing, and that trace aptamer contamination from the laboratory environment was not significantly contributing to the signal (a perpetual consideration for aptamer analysis by qPCR). To test this, we synthesized pure stocks of aptamers A, B, E, and X. Ten mice were injected with 200 pmol of an aptamer cocktail (50 pmol each of A, B, E, and X) or vehicle (Supplementary Fig. S3A). Mice were randomly assigned with blinding to receive either aptamer cocktail or vehicle. Mice were euthanized 4 h post-injection, and organs were again thoroughly perfused prior to harvest. Aptamers were extracted and quantified by qPCR using sequence-specific primers (Supplementary Table S2 and Supplementary Fig. S3B and C). In attempts to limit PCR sequence bias, primers were designed such that the PCR efficiency of any candidate was never greater than that of the negative control sequence, X (Supplementary Fig. S3B and C). Recovered aptamer signal

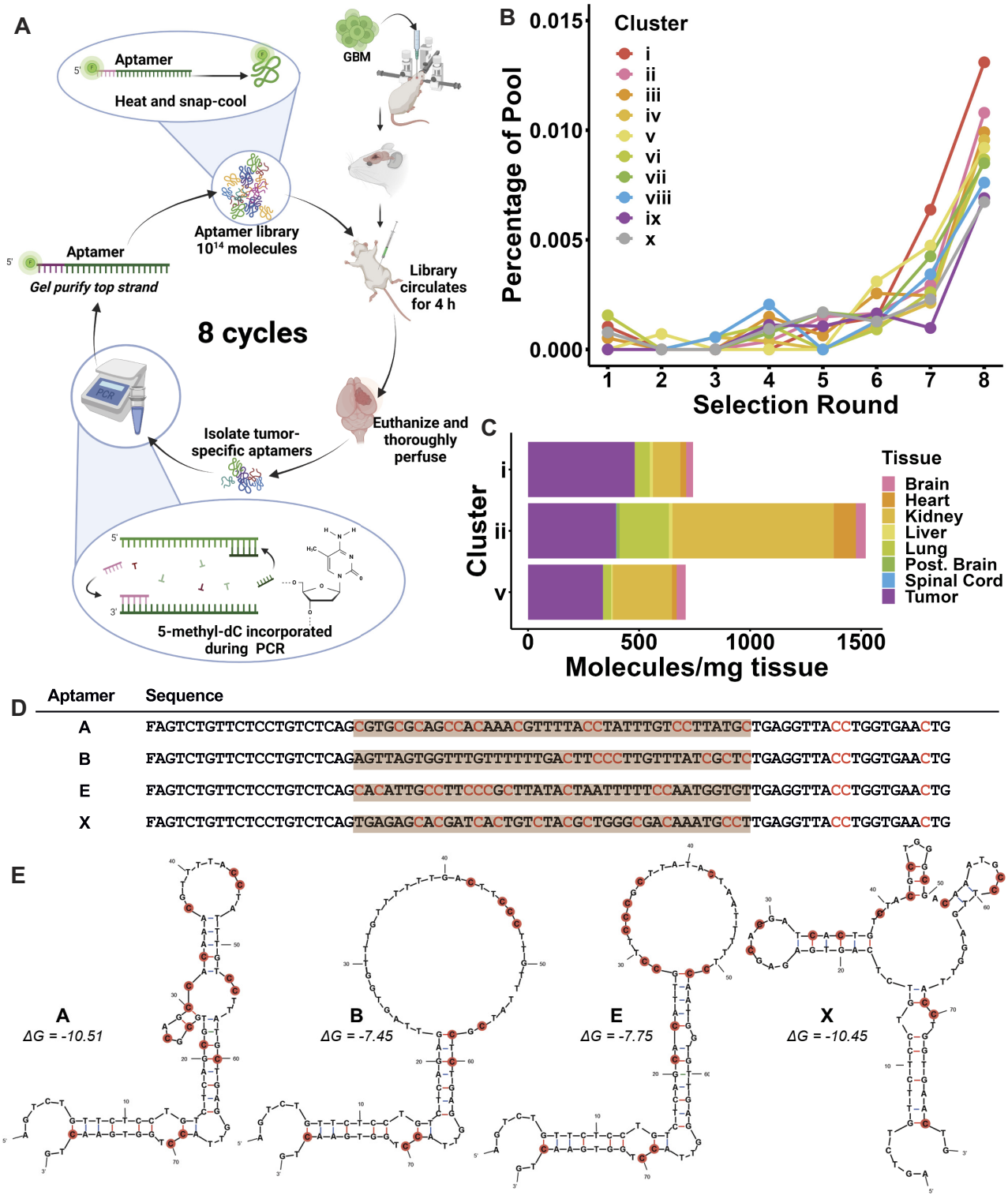

Figure 1. *In vivo* SELEX selecting PDX GBM-specific DNA aptamers in mice. (**A**) Schematic diagram of *in vivo* SELEX protocol applied to an orthotopic GBM39-eGFP-FLUC2 PDX model. Green "F" in aptamer depiction represents fluorescein. (**B**) Deep sequencing results identifying the 10 most enriched 80-mer DNA aptamer sequence clusters over eight rounds of selection. (**C**) Biodistribution of the indicated aptamer sequence clusters among the indicated tissues was determined from deep sequencing data after 4 h for three dominant aptamer sequence clusters observed at round 8. "Post. Brain": posterior brain. (D) Aptamer sequences selected for study. Gray shading indicates sequences arising from the random region of the DNA library. F: fluorescein; red: 5-methyl-dC. Negative control (X) was selected at random from sequences present in the naïve library but not found in round 8. (**E**) Secondary structures of selected aptamer candidates and negative control as predicted by Mfold software for 153 mM Na^+ and 1 mM Mg^{2+} at 24°C. Estimated ΔG values for folding stabilities are in kJ/mol. Highlighted cytosines: 5-methyl-dC.

was much higher than background vehicle signal in all organ extracts, indicating minimal laboratory background contamination (Supplementary Fig. S5A–C). Further, background vehicle signal did not increase over the 10 sequentially aptamer-dosed mice, demonstrating avoidance of animal-to-animal cross-contamination.

Biodistribution of aptamer candidates

We quantified the biodistribution of aptamer candidates relative to a negative control aptamer X using qPCR with aptamer-specific primers and appropriate standard curves. To understand biodistribution in the brain, frozen specimens were dissected as shown in Fig. 2A. The posterior left hemisphere and cerebellum were similarly dissected. The 1-mm tumor section was shown to be representative of the entire tumor (Supplementary Fig. S5D and E). All three aptamer candidates accumulated in the GBM tumor significantly above the background levels detected in vehicle-injected mice, and above the levels of the negative control aptamer present in the tumor (Fig. 2B). By qPCR, aptamers A, B, and E accumulated to an average of 11.4 ± 5.1 million aptamers/mg tumor tissue, compared to 2.1 ± 0.9 million aptamers/mg for negative control X (Fig. 2B). Aptamer accumulation in adjacent lateral, nontumor tissue was low and comparable for aptamer A and negative control X (Fig. 2C). While aptamers B and E were detected at higher levels in this nontumor brain tissue, their levels were still >10-fold lower per mg of tissue than levels accumulated in the tumor. Samples from normal brain in the contralateral left hemisphere, distant from the tumor, showed all aptamer levels to be comparable to negative control X. Results from analysis of the cerebellum were similar (Fig. 2C). Taken together, these data demonstrate that the three *in vivo*-selected candidate aptamers demonstrate significant GBM tumor homing in brain.

For all three candidates, significantly higher aptamer levels were detected in the tumor as compared to the adjacent brain, bone marrow, cerebellum, heart, kidney, liver, lung, posterior left-brain hemisphere, and sciatic nerve, again demonstrating tumor homing (Fig. 2D and Supplementary Fig. S5C). When the data were analyzed by aptamer biodistribution across the four individual mice that received aptamer cocktail, tumor-homing preference remained evident, a feature not observed for negative control aptamer X (Fig. 2E). Importantly, similar results were obtained for these animals representing two different experiments done at two separate times (Supplementary Fig. S3C).

Aptamer enrichment is not a result of enhanced serum stability

A potential selective pressure on *in vivo* SELEX DNA libraries in circulation for several hours is serum stability, favoring nuclease-resistant sequences and conformations. To elucidate whether serum stability was included as selection criteria, aptamers were incubated at 37°C in 100% FBS. Aliquots were removed and qPCR, which only detects fully intact molecules, was used to detect degradation. The half-lives in 100% FBS for aptamers A, B, E, and X were calculated to be 1.0, 1.2, 0.5, and 1.3 h, respectively (Fig. 3A). Surprisingly, aptamer E was the only aptamer whose stability was notably different from the naïve library, in this case lower. Thus, DNA candidates selected for GBM homing after eight rounds of *in vivo* SELEX had not developed nuclease resistance.

Despite the relatively short, calculated half-lives of aptamers in 100% FBS, additional confirmation of the presence of aptamers in the orthotopic brain tumor was sought. Fluorescence microscopy was used to detect GBM-specific aptamers in the tumor 4 h post-injection by exploiting the 5′-FAM present on all molecules. Mice received 250 pmol of either aptamer E or X. After 4 h, mice were euthanized and thoroughly perfused as usual. Brains from these mice were frozen and serial sections prepared for slide mounting, DAPI staining, and imaging with confocal microscopy to detect 5′-FAM-labeled aptamer signal (Fig. 3B). Strikingly, for mice injected with aptamer E, fluorescent signal was strongly evident, penetrating the parenchyma of the brain tumor. In contrast, minimal aptamer signal was detected in the normal brain hemisphere. The brain of the mouse injected with negative control aptamer X showed minimal fluorescence in the brain parenchyma or the tumor (Fig. 3B). These data confirm that *in vivo*-selected aptamers exit circulation and penetrate tumor tissue, despite their relatively rapid decay in serum.

Selectivity of aptamers for tumor relative to brain

Although the aptamers were homing to the tumor, the cell specificity of candidate aptamers was unknown. Given the complexity of PDX models and the propensity of PDX cultured cells to evolve in culture, aptamer–GBM39 tumor cell association was first tested histologically in the brains of aptamer-untreated parental GBM39 (lacking eGFP) PDX mice. Brains were fixed, paraffin embedded, and serially sectioned. Using an immunofluorescence protocol to detect aptamers with labeled anti-FAM antibodies, brain sections were treated with 200 nM aptamer, DAPI, and were imaged using confocal microscopy. Tumor-specific signal was observed for aptamer E, but not aptamer X (Fig. 4). Not only does this result confirm the specificity of aptamer E, but it also suggests the possible application of aptamers for histopathology or diagnostic uses.

Selectivity of candidate aptamers in cell culture

Biodistribution experiments suggest that *in vivo*-selected aptamers bind one or more GBM tumor-specific targets. Whether aptamers were staining PDX target cells or binding nontumor cells or other ligands in the tumor microenvironment was unknown. To elucidate this, explants of parental GBM39 cells (lacking eGFP) were cultured *in vitro* and exposed to 200 nM aptamer in wash buffer with sheared salmon sperm DNA competitor for 1 h followed by washing and imaging. Aptamers A and E demonstrated significant binding to GBM39 cells in culture (Fig. 5A and B), but no binding above negative control levels was observed for aptamer B either by microscopy or by qPCR. This result suggests that aptamers A and E recognize GBM39 cell features in the PDX tumor, while aptamer B may have been selected for recognition of some other feature in the tumor microenvironment.

Interestingly, aptamers A and E synthesized without 5-methyl-dC substitution lost the ability to bind GBM39 cells in culture. This result suggests that cytosine methylation plays a role in stabilizing aptamer tertiary folding and/or target binding (Supplementary Fig. S6).

In vitro culture of many GBM PDX lines, including GBM39, is complicated by variations in cell behavior. GBM39 is propagated by growth as flank tumors passaged between

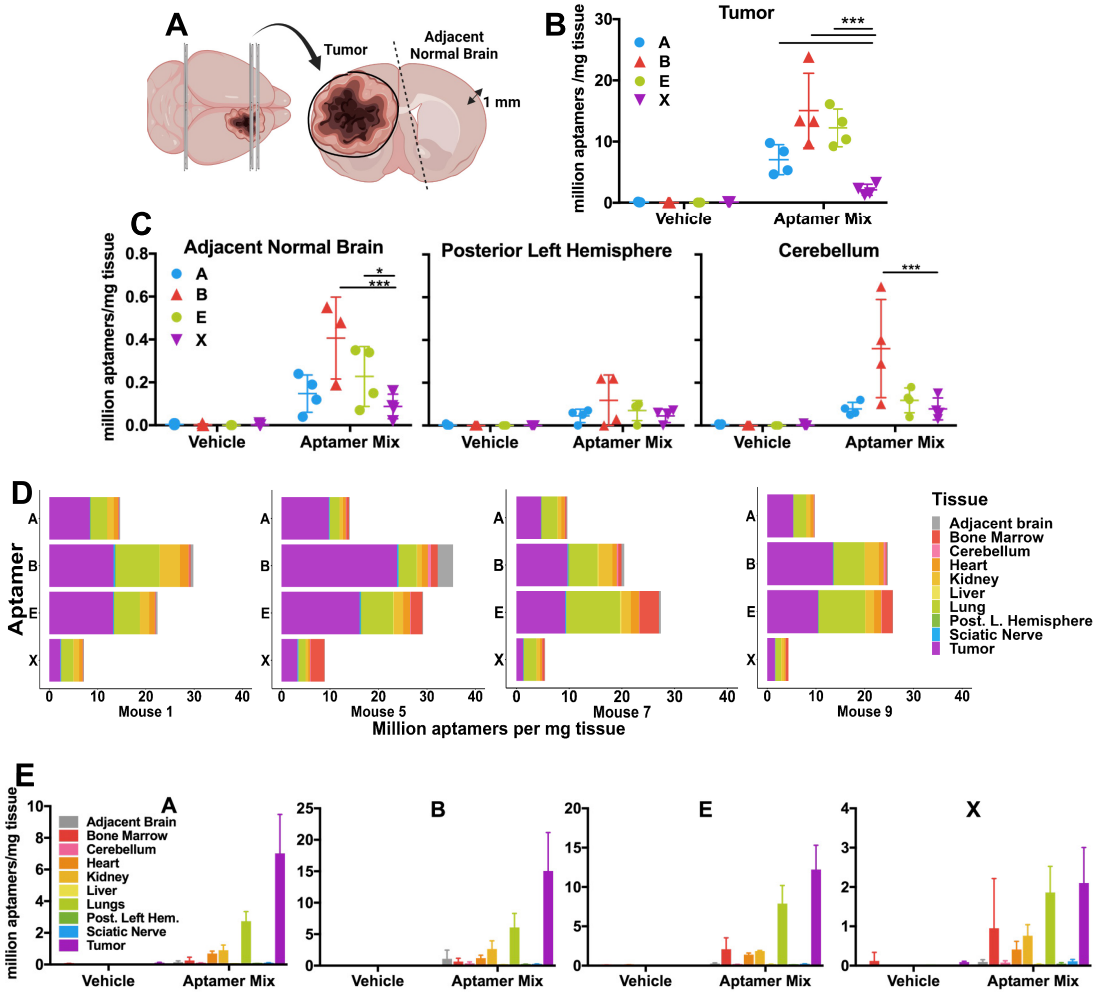

Figure 2. *In vivo* biodistribution of aptamers A, B, and E relative to negative control X. Mice were injected i.p. with either placebo PBS solution lacking aptamers or 200 pmol of a mixture of aptamers A, B, E, and X (50 pmol each). Mice were euthanized after 4 h, subjected to thorough perfusion with PBS, aptamers extracted from the indicated tissues, and quantified by qPCR. (**A**) Tissue specimens from orthotopic xenograft GBM tumor versus adjacent brain regions were identified by toluidine blue staining and collected in 1-mm slices. (**B**) Aptamer yields from the GBM39 GBM brain tumor of four mice demonstrating the range of yields and absence of aptamer contamination during handling. (**C**) Aptamer detection in nontumor locations of the brain in mice that received vehicle or aptamer mixtures. Biodistribution of aptamers in mice injected with aptamer mixture indicated by animal (**D**) or by aptamer (**E**). All qPCR samples were analyzed in technical triplicates. $*P < .05$; $**P < .01$, and $***P < .001$ by two-sided *t*-test.

mice. A small fraction of such cells is seeded for adherent cell culture studies but can be passaged only once, complicating the generation of replicate data. Interestingly, the cell staining shown in Fig. 5A was observed repeatedly for GBM39 explants between 24 and 72 h post-seeding. However, binding to cells in culture was lost a few passages later. Reassuringly, when later GBM39 passages were orthotopically implanted in mice, aptamer *in vivo* tumor-homing preference was consistent. This suggests that levels of expression of ligands for aptamers A and E may be variable *in vitro* and more prominent in the context of the orthotopic tumor microenvironment in the brain.

The inherent toxicity of *in vivo*-selected aptamers for GBM39 cells was tested (Fig. 5C). None of the three *in vivo*-selected candidates nor the negative control was detectably toxic to the GBM39 in culture. This suggests that aptamers A, B, and E demonstrate a safety profile compatible with eventual GBM theranostic use.

Specificity of candidate aptamers for other human cells in culture

Aptamers were selected *in vivo* using xenografts, suggesting the possibility that they retain selectivity for nonspecific human or tumor-specific antigens. We tested cell binding of aptamer candidates to multiple GBM cell lines as well as non-GBM cells (Fig. 6). Results for each independent experiment were normalized to results for negative control aptamer X to account for any cell culture variability. Aptamers A, B, and E only detectably bound to GBM39 and no other GBM human cell lines (U87) or PDX models (GBM14 or GBM43) tested in culture. The aptamers also demonstrated minimal binding to other non-GBM human cell lines (MCF7, A549, HeLa, U2OS, and SVG-A; Fig. 6). Taken together, these results suggest that *in vivo*-selected anti-GBM aptamers bind to GBM39-specific tumor antigens that are not upregulated on other human cancer cells and are not simply distinguishing human from mouse cells.

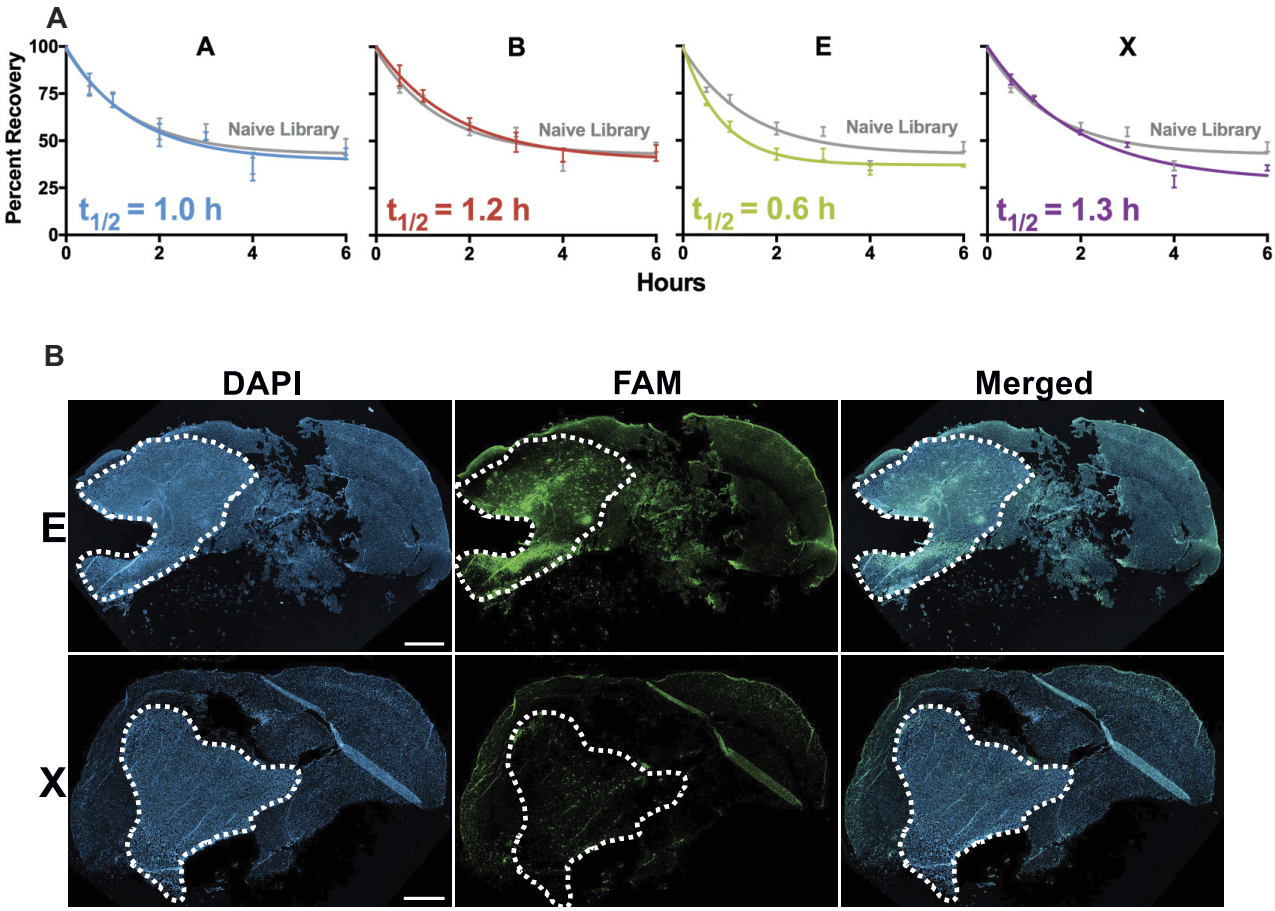

Figure 3. Aptamer serum stabilities and *in vivo* distribution of aptamer E relative to negative control X. (**A**) Aptamer serum stability in 100% FBS at 37°C determined by qPCR. Fits show first-order decay curves and deduced half-lives. (**B**) Fluorescent aptamer detection in GBM orthotopic xenograft mouse brain after i.p. injection of 250 pmol aptamer E or X, euthanasia after 4 h, and thorough perfusion with PBS. Whole brains were dissected and frozen in OCT. Five-micrometer sections of frozen brain were stained with DAPI and then imaged and tiled using confocal fluorescence microscopy. Aptamers were detected by their 5′-FAM labels. Scale bar is 1 mm.

Discussion

More than two decades of failed GBM clinical trials and unimproved prognoses are irrefutable evidence that human engineered drug design has yet to yield an improved therapeutic strategy for GBM. Here, we describe the first example applying the principles of natural selection via *in vivo* SELEX with an orthotopic PDX brain tumor mouse model to identify DNA aptamers capable of homing to a human GBM (GBM39). Just eight selection rounds were required to identify aptamers from a vast random library of ~100 trillion unique sequences for the ability to localize to the brain tumor within 4 h of i.p. injection. This capability was confirmed by multiple independent methods. These findings suggest that *in vivo* SELEX is a viable strategy for developing GBM diagnostics and homing agents that might eventually be formulated as drug conjugates.

In the planning of our approach, DNA molecules were selected instead of modified RNA molecules due to the differences in plasma stability, the cost of manufacturing, and the ease of aptamer SELEX preparation in the context of timed *in vivo* tumor development [24]. As a result, we considered that DNA aptamers have the potential to be detected by two "danger" response systems of the mammalian innate immune system. Though unlikely to affect results over the short 4-h window of our experiments, toll-like receptor 9 (TLR9) can detect unmethylated 5′-CpG motifs in DNA as a pathogen-associated molecular pattern (PAMP) [25]. Wishing to avoid effects of potential complicating TLR9-based innate immune responses to DNA aptamer libraries sensed as PAMPs, all libraries and individual aptamers were prepared such that any 5′-CpG dinucleotides contained 5-methyl-dC. In addition, we note that the cGAS–STING pathway is known to trigger innate immune responses to cytoplasmic DNA sensed as evidence of pathogenic activity or cellular damage [26]. However, interferon production by the cGAS–STING system is thought to be most sensitive to relatively long double-stranded DNA fragments (unlike the aptamers present in our libraries) [26]. Future studies will address whether DNA aptamer libraries of the form used here have any potential to trigger the cGAS–STING pathway of innate immunity over longer time periods.

The current proof-of-concept experiments were deliberately performed using a PDX characterized by a relatively permeable BBB to enhance the likelihood of identifying anti-GBM aptamers capable of tumor penetration [8]. In the healthy intact BBB, the extensive presence of tight junctions and adherens junctions on endothelial cells restricts most macromolecules from utilizing paracellular transport [27]. Thus, the transcytosis of macromolecules relies on transcellular pathways such as carrier-mediated or receptor-mediated transcytosis [27]. Some therapies have been designed to

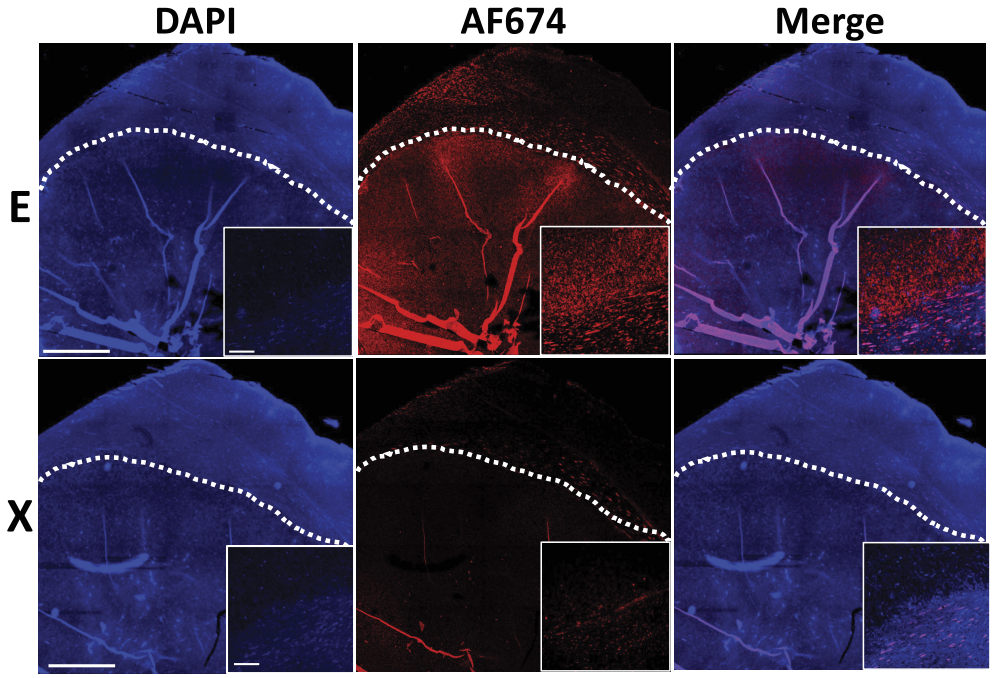

Figure 4. Aptamer staining of mouse brain bearing GBM39 PDX tumor. Serial sections of fresh-frozen untreated mouse brain embedded in OCT were stained with the indicated candidate aptamers or negative control and imaged by confocal microscopy. Composite images show tumor stained with aptamer E versus X. Insets show higher magnification of the tumor–normal brain interface. Scale bars are 1 mm and 200 μm, respectively.

exploit endogenous receptor-mediated transcytosis proteins, such as transferrin, to permit macromolecules or nanoparticles to penetrate the BBB [28, 29]. This is compounded by the establishment of an orthotopic xenograft, which requires disruption of the BBB by stereotactic injection, leaving the integrity of the BBB in xenograft models questionable [30]. However, in previous studies testing ADCs in patient-derived orthotopic xenograft models, the leakiness established by the PDX explants directly correlated with (i) the accumulation and (ii) the efficacy of the ADC. Additionally, surgical resection remains an important determinant of GBM patients' overall survival [31, 32]. We hypothesize that stereotactic injection of the PDX explant cells in mice and surgical resection of the GBM tumor in humans disrupt the BBB similarly making this a useful model for developing tumor-homing aptamers. Thus, how aptamers A, B, and E cross the BBB is unknown, but *in vivo* SELEX has previously been used to select aptamers against the normal mouse brain parenchyma, thus establishing that some aptamers can penetrate the BBB [9]. The GBM PDX model used in our studies has a relatively permeable BBB to ADCs that likely facilitated aptamer candidate identification in eight selection rounds [8]. However, the selected aptamers accumulate on average ~5-fold higher in the GBM compared to the negative control aptamer, indicating that BBB permeability and associated diffusion alone does not explain the tumor-homing characteristics observed for the selected aptamers. Future studies will test various alternative PDX models characterized by a predictable range of BBB permeabilities.

Our studies reproducibly confirm the *in vivo* tumor-homing capability of three candidate DNA aptamers compared to a negative control aptamer. Levels of aptamer accumulated in the tumor were ~10–100-fold higher than those in adjacent normal brain tissue. Strikingly, the candidate aptamers were also selective for the PDX tumor relative to other organs, demonstrating tumor-homing preference. We note that the biodistribution across nontumor organs differed somewhat between the complex DNA aptamer library studied in the round 8 selection mouse and when the four candidate DNA aptamers were combined for biodistribution experiments. A contributing factor was undoubtedly the optimized aptamer extraction method introduced for more reliable and reproducible biodistribution measurements. This optimized method is recommended for future *in vivo* SELEX experiments.

After measuring *in vivo* biodistribution, we sought to understand whether *in vivo* selection results in aptamers with increased serum stabilities. This was not the case. Randomly chosen (unselected) aptamer E had a somewhat shorter half-life relative to the naïve DNA library in 100% FBS, as detected by qPCR. However, even traces of aptamer E were detectable by microscopy in the tumor 4 h post-injection, indicating that DNA aptamers exit circulation and penetrate into the tumor despite their relative instability in serum.

Our *in vivo* SELEX protocol identifies DNA aptamers that associate with GBM orthotopic PDX brain tumors. These tumors are known to constitute a heterogeneous mixture of human GBM cells in the context of mouse stromal cells, immune cells, and vasculature, creating the potential for aptamer selection to occur against nonspecific human antigens or even tumor microenvironment-associated mouse antigens. Therefore, aptamers were tested *in vitro* for binding to the cultured target GBM39 PDX line. Indeed, aptamers A and E bound to these target cells but not other human tumor cells in culture. Aptamer B failed to strongly bind the target GBM line or other human tumor cells, suggesting an alternative tumor-associated target. None of the three candidate DNA aptamers were toxic to GBM39 cells *in vitro* suggesting that these candidates may have promise for therapeutic delivery or diagnostic purposes.

Interestingly, the most promising aptamers selected, A and E, were quite specific to the target line, G39, with aptamer

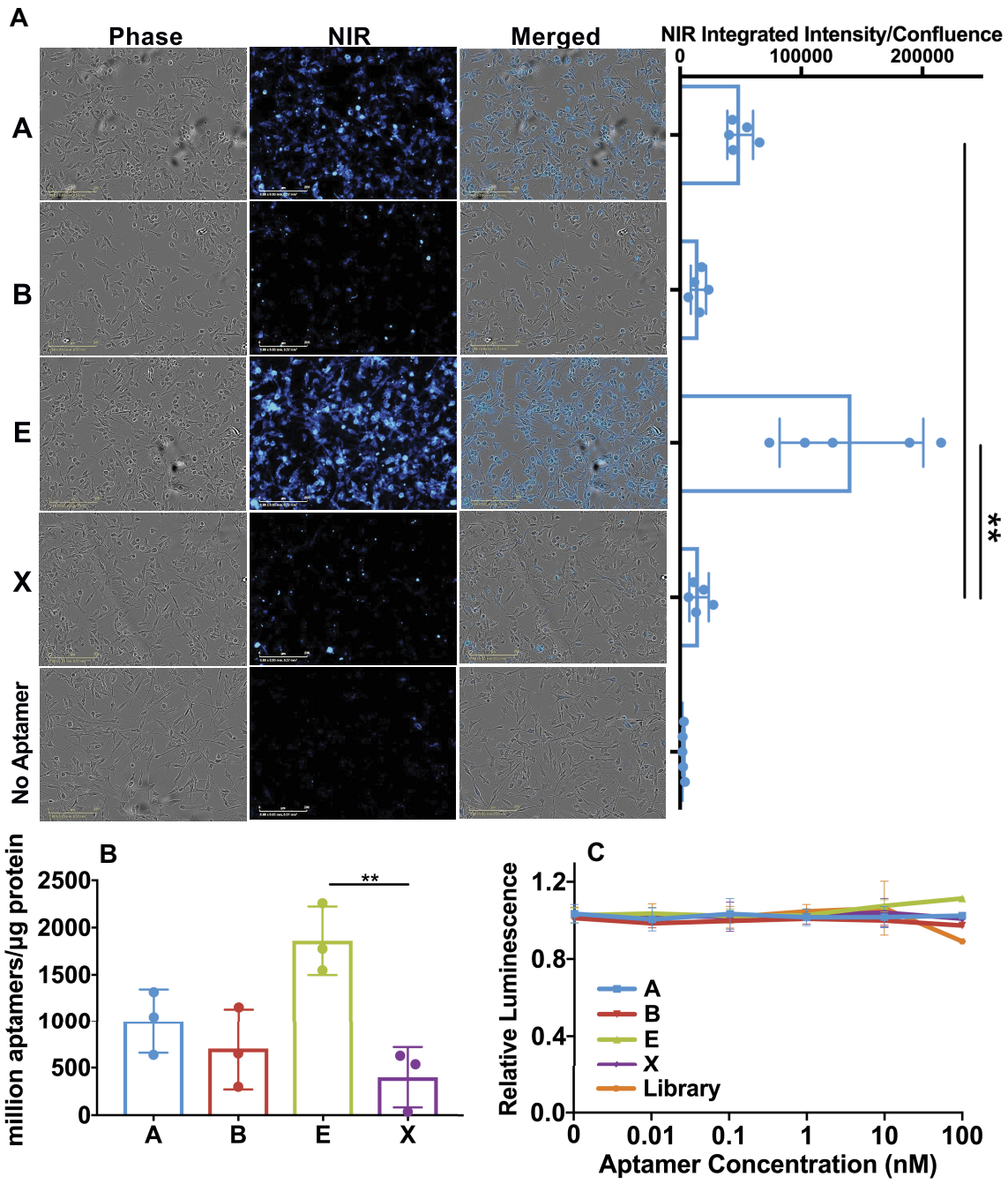

Figure 5. Quantitation of *in vitro* binding of *in vivo*-selected aptamers to cultured GBM39 GBM cells. Aptamers (200 nM) were incubated with cultured cells for 1 h, washed, and cell association determined by (**A**) live cell imaging and (**B**) qPCR, as described in the "Materials and methods" section. (**C**) CellTiter-Glo assay demonstrating lack of aptamer candidate toxicity on GBM39 cells. $^{**}P < .01$ by two-sided *t*-test.

E unable to recognize other GBM lines tested in cell culture. However, we acknowledge that this is by no means a comprehensive GBM panel and is limited to the cell lines and PDX explants tested in cell culture. The orthotopic environment also impacts the antigens on the cell surface and it is unknown whether the aptamers selected would bind and recognize U87, G14, or G43 in the *in vivo* setting. Uniquely, aptamer identification by SELEX "probes" the upregulated tumor antigens in the *in vivo* setting. It must be acknowledged that this may not be reflected accurately of cells in culture. Second, it is possible that the specificity of the aptamers identified in this *in vivo* SELEX speaks to the heterogeneity of the GBM cell population and illustrates the necessity to develop GBM targeting moieties against multiple—if not a library of—GBM tumor antigens. Thus, future work should build upon this finding by selecting aptamers across multiple models or using a toggle-SELEX approach.

This work provides the first demonstration of *in vivo* selection in the context of an orthotopic PDX GBM model. This approach can, in principle, be applied to other tumors where conventional therapies are ineffective and novel agents are needed. Applications involving toxin conjugates might be addressed by either selections using pre-conjugated random libraries or post-conjugation strategies after selection. We

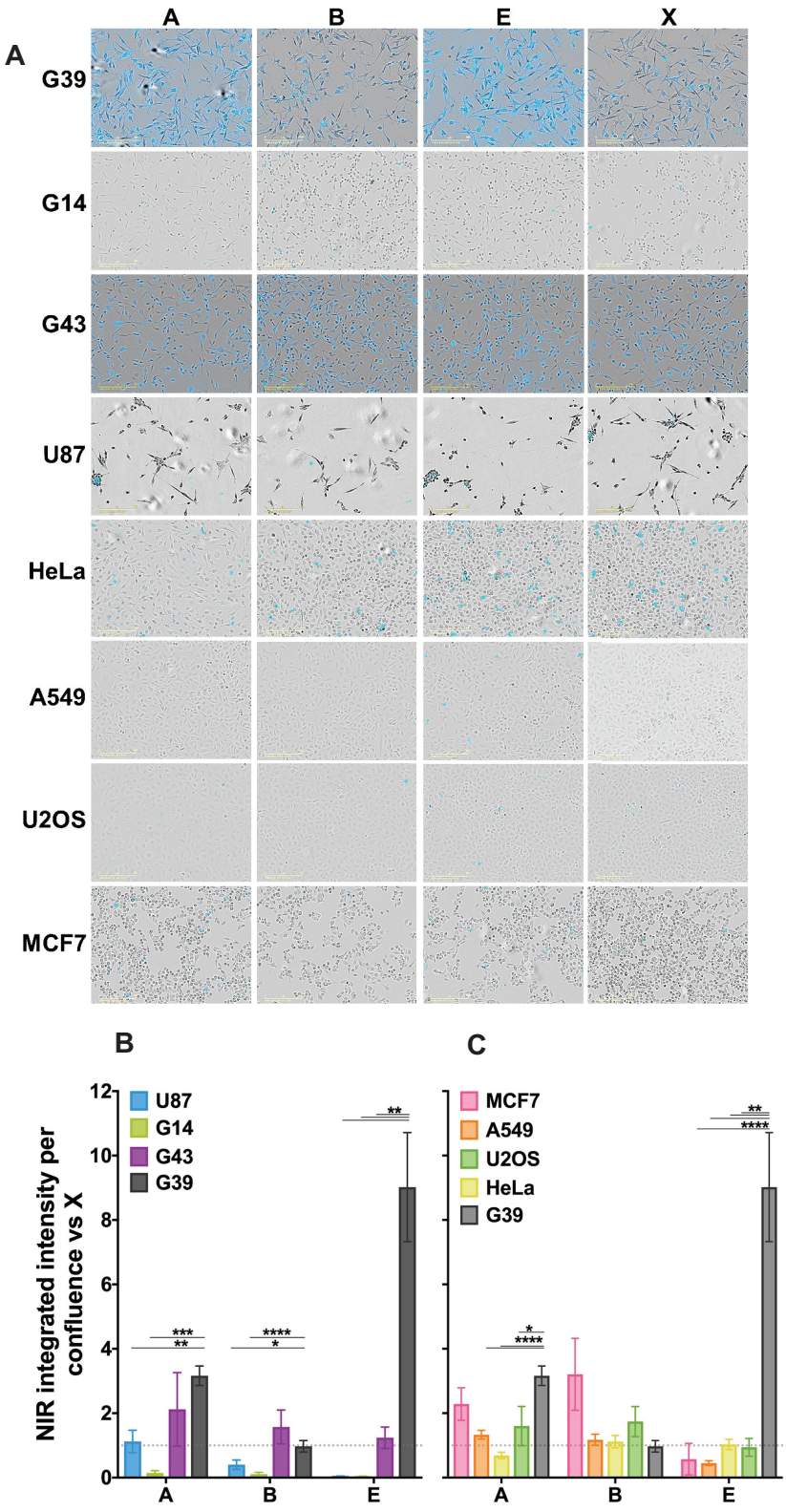

Figure 6. *In vitro* characterization of anti-GBM aptamer association with various cell lines. (**A**) Aptamers were incubated with cells for 1 h, washed, and cell association determined by imaging. (**B**) Quantitation as near-infrared (NIR) integrated intensity per confluence relative to negative control aptamer X for the indicated cultured GBM cell lines. (**C**) Quantitation for the indicated non-GBM cell lines. Two-sided *t*-tests were completed comparing the relative binding of an aptamer in G39 to the same aptamer in a different cell line. $*P < .05$; $**P < .01$, $***P < .001$, and $****P < .0001$.

conclude that *in vivo* SELEX can be used as a method for developing unmodified DNA aptamers as a platform for novel theranostics.

Acknowledgements

Author contributions: Conceptualization by L.J.M., J.N.S., C.D.D., and B.A.W.; Funding acquisition by J.N.S. and L.J.M.; Data Curation, Formal Analysis, Investigation, and Validation by C.D.D., S.J., K.K.B., B.A.W., K.S.P., and N.W.L.; Methodology by J.N.S., L.J.M, C.D.D., S.J., B.A.W., K.S.P., and D.M.B.; Project administration by D.M.B; Writing – original draft by C.D.D.; Writing – review & editing by C.D.D., L.J.M., B.A.W., and J.N.S.

Supplementary data

Supplementary data is available at NAR Cancer online.

Conflict of interest

None declared.

Funding

This work was supported by Mayo Clinic (L.J.M. and J.N.S); L.J.M. is the Bernard Pollack Professor and J.N.S. is the William H. Donner Professor at Mayo Clinic. This work was also supported by NIH grants T32GM145408 Mayo Clinic Medical Scientist Training Program (C.D.D.), R35GM143949 (L.J.M.), and R61NS128071-01A1 (J.N.S. and L.J.M.), Mayo Clinic CTSA grant UL1TR000135, a Mayo Clinic CCaTS-CBD Team Science award, a generous grant from the Humor to Fight the Tumor Foundation, and an NSF graduate fellowship (B.A.W.).

Data availability

All data are provided in supplementary materials. Constructs are available from the authors upon request.

References

1. Ostrom QT, Price M, Neff C *et al.* CBTRUS Statistical Report: primary brain and other central nervous system tumors diagnosed in the United States in 2016–2020. *Neuro Oncol* 2023;**25**:iv1–99. https://doi.org/10.1093/neuonc/noad149
2. Ah-Pine F, Khettab M, Bedoui Y *et al.* On the origin and development of glioblastoma: multifaceted role of perivascular mesenchymal stromal cells. *Acta Neuropathol Commun* 2023;**11**:104. https://doi.org/10.1186/s40478-023-01605-x
3. Fisher JP, Adamson DC. Current FDA-approved therapies for high-grade malignant gliomas. *Biomedicines* 2021;**9**:324. https://doi.org/10.3390/biomedicines9030324
4. McFaline-Figueroa JR, Wen PY. Negative trials over and over again: how can we do better? *Neuro Oncol* 2023;**25**:1–3. https://doi.org/10.1093/neuonc/noac226
5. Steeg PS. The blood–tumour barrier in cancer biology and therapy. *Nat Rev Clin Oncol* 2021;**18**:696–714. https://doi.org/10.1038/s41571-021-00529-6
6. Arvanitis CD, Ferraro GB, Jain RK. The blood–brain barrier and blood–tumour barrier in brain tumours and metastases. *Nat Rev Cancer* 2020;**20**:26–41. https://doi.org/10.1038/s41568-019-0205-x
7. Becker AP, Sells BE, Haque SJ *et al.* Tumor heterogeneity in glioblastomas: from light microscopy to molecular pathology. *Cancers* 2021;**13**:761. https://doi.org/10.3390/cancers13040761
8. Marin B-M, Porath KA, Jain S *et al.* Heterogeneous delivery across the blood–brain barrier limits the efficacy of an EGFR-targeting antibody drug conjugate in glioblastoma. *Neuro Oncol* 2021;**23**:2042–53. https://doi.org/10.1093/neuonc/noab133
9. Cheng C, Chen YH, Lennox KA *et al. In vivo* SELEX for identification of brain-penetrating aptamers. *Mol Ther Nucleic Acids* 2013;**2**:e67. https://doi.org/10.1038/mtna.2012.59
10. Hermann T, Patel DJ. Adaptive recognition by nucleic acid aptamers. *Science* 2000;**287**:820–5. https://doi.org/10.1126/science.287.5454.820
11. Ng EWM, Shima DT, Calias P *et al.* Pegaptanib, a targeted anti-VEGF aptamer for ocular vascular disease. *Nat Rev Drug Discov* 2006;**5**:123–32. https://doi.org/10.1038/nrd1955
12. Moshfeghi AA, Puliafito CA. Pegaptanib sodium for the treatment of neovascular age-related macular degeneration. *Expert Opin Investig Drugs* 2005;**14**:671–82. https://doi.org/10.1517/13543784.14.5.671
13. Jin C, Qiu L, Li J *et al.* Cancer biomarker discovery using DNA aptamers. *Analyst* 2016;**141**:461–6. https://doi.org/10.1039/C5AN01918D
14. Fechter P, Cruz Da Silva E, Mercier M-C *et al.* RNA aptamers targeting integrin $\alpha5\beta1$ as probes for cyto- and histofluorescence in glioblastoma. *Mol Ther Nucleic Acids* 2019;**17**:63–77. https://doi.org/10.1016/j.omtn.2019.05.006
15. Doherty C, Wilbanks B, Khatua S *et al.* Aptamers in neuro-oncology: an emerging therapeutic modality. *Neuro Oncol* 2024;**26**:38–54. https://doi.org/10.1093/neuonc/noad156
16. Klußmann S, Nolte A, Bald R *et al.* Mirror-image RNA that binds D-adenosine. *Nat Biotechnol* 1996;**14**:1112–5. https://doi.org/10.1038/nbt0996-1112
17. Roccaro AM, Sacco A, Purschke WG *et al.* SDF-1 inhibition targets the bone marrow niche for cancer therapy. *Cell Rep* 2014;**9**:118–28. https://doi.org/10.1016/j.celrep.2014.08.042
18. Giordano FA, Layer JP, Leonardelli S *et al.* L-RNA aptamer-based CXCL12 inhibition combined with radiotherapy in newly-diagnosed glioblastoma: dose escalation of the phase I/II GLORIA trial. *Nat Commun* 2024;**15**:4210.https://doi.org/10.1038/s41467-024-48416-9
19. Carlson BL, Pokorny JL, Schroeder MA *et al.* Establishment, maintenance, and *in vitro* and *in vivo* applications of primary human glioblastoma multiforme (GBM) xenograft models for translational biology studies and drug discovery. *Curr Protoc Pharmacol* 2011;**52**:14.16.1–23. https://doi.org/10.1002/0471141755.ph1416s52
20. Vaubel RA, Tian S, Remonde D *et al.* Genomic and phenotypic characterization of a broad panel of patient-derived xenografts reflects the diversity of glioblastoma. *Clin Cancer Res* 2020;**26**:1094–104. https://doi.org/10.1158/1078-0432.CCR-19-0909
21. Hoinka J, Backofen R, Przytycka TM. AptaSUITE: a full-featured bioinformatics framework for the comprehensive analysis of aptamers from HT-SELEX experiments. *Mol Ther Nucleic Acids* 2018;**11**:515–7. https://doi.org/10.1016/j.omtn.2018.04.006
22. Zuker M. Mfold web server for nucleic acid folding and hybridization prediction. *Nucleic Acids Res* 2003;**31**:3406–15. https://doi.org/10.1093/nar/gkg595
23. SantaLucia J. A unified view of polymer, dumbbell, and oligonucleotide DNA nearest-neighbor thermodynamics. *Proc Natl Acad Sci USA* 1998;**95**:1460–5. https://doi.org/10.1073/pnas.95.4.1460
24. Bernhardt HS, Tate WP. Primordial soup or vinaigrette: did the RNA world evolve at acidic pH? *Biol Direct* 2012;**7**:4. https://doi.org/10.1186/1745-6150-7-4
25. Bauer S, Kirschning CJ, Häcker H *et al.* Human TLR9 confers responsiveness to bacterial DNA via species-specific CpG motif recognition. *Proc Natl Acad Sci USA* 2001;**98**:9237–42. https://doi.org/10.1073/pnas.161293498

26. Motwani M, Pesiridis S, Fitzgerald KA. DNA sensing by the cGAS–STING pathway in health and disease. *Nat Rev Genet* 2019;**20**:657–74. https://doi.org/10.1038/s41576-019-0151-1
27. Wu D, Chen Q, Chen X *et al.* The blood–brain barrier: structure, regulation and drug delivery. *Signal Transduct Target Ther* 2023;**8**:217. https://doi.org/10.1038/s41392-023-01481-w
28. Zhou Q-H, Boado RJ, Lu JZ *et al.* Monoclonal antibody-glial-derived neurotrophic factor fusion protein penetrates the blood–brain barrier in the mouse. *Drug Metab Dispos* 2010;**38**:566–72. https://doi.org/10.1124/dmd.109.031534
29. Thomsen MS, Johnsen KB, Kucharz K *et al.* Blood–brain barrier transport of transferrin receptor-targeted nanoparticles. *Pharmaceutics* 2022;**14**:2237. https://doi.org/10.3390/pharmaceutics14102237
30. Genovesi LA, Puttick S, Millar A *et al.* Patient-derived orthotopic xenograft models of medulloblastoma lack a functional blood–brain barrier. *Neuro Oncol* 2021;**23**:732–42. https://doi.org/10.1093/neuonc/noaa266
31. Brown NF, Ottaviani D, Tazare J *et al.* Survival outcomes and prognostic factors in glioblastoma. *Cancers* 2022;**14**:3161. https://doi.org/10.3390/cancers14133161
32. Kartik R, Lee GR, Lee CC *et al.* Clinical prognostic factors of survival in glioblastoma multiforme. *Neurology* 2020;**94**:2593. https://doi.org/10.1212/WNL.94.15_supplement.2593

Received: October 24, 2024. **Revised:** January 24, 2025. **Editorial Decision:** January 29, 2025. **Accepted:** February 3, 2025